Journal of Statistical Mechanics:
Theory and Experiment

PAPER: CLASSICAL STATISTICAL MECHANICS, EQUILIBRIUM AND NON-EQUILIBRIUM

The role of dynamic defects in transport of interacting molecular motors

Journal of Statistical Mechanics: Theory and Experiment
An IOP and SISSA journal

PAPER: Classical statistical mechanics, equilibrium and non-equilibrium

The role of dynamic defects in transport of interacting molecular motors

Akriti Jindal[1], Anatoly B Kolomeisky[2] and Arvind Kumar Gupta[1]

[1] Department of Mathematics, Indian Institute of Technology Ropar, Rupnagar-140001, Punjab, India
[2] Department of Chemistry and Chemical and Biomolecular Engineering, Rice University, Houston, TX 77005, United States of America
E-mail: akgupta@iitrpr.ac.in

Received 13 November 2019
Accepted for publication 30 January 2020
Published 14 April 2020

Online at stacks.iop.org/JSTAT/2020/043206
https://doi.org/10.1088/1742-5468/ab7756

Abstract. Motor proteins or biological molecular motors are special enzyme molecules that drive biological transport in living cells by moving cellular cargoes along linear protein filaments. The experimental evidences suggest that while performing their mechanical work biological molecular motors interact with each other, and there are other biological molecules on their tracks that influence their progression. Stimulated by these observations, we propose a one-dimensional totally asymmetric simple exclusion process with nearest-neighbor interactions and a dynamic defect that is allowed to reversibly bind and unbind at a specific site far away from the boundaries. A theoretical framework based on cluster mean-field approximation is adopted to determine the stationary properties of the system. The role of interactions and the effect the reversible defect associations on the dynamics of the system is discussed. It is found that three or less stationary phases can exist in the system, depending on the interaction strength, and only one of them is strongly affected by the defect association/dissociation dynamics. The theoretical results are validated through extensive Monte Carlo simulations.

Keywords: driven diffusive systems, exclusion processes, molecular motors, traffic models

1742-5468/20/043206+20$33.00

Contents

1. Introduction **2**

2. Definition of the model **4**

3. Mathematical description of the model **6**
3.1. Two-site CMF approximation for TASEP with interacting particles.....7
3.2. Defect dynamics 8

4. Stationary phase diagrams **10**
4.1. HD/LD phase 10
4.2. LD/LD phase.....11
4.3. HD/HD phase.....11
4.4. LD/HD phase 12
4.5. MC/MC phase.....12

5. Results and discussions **13**
5.1. Effect of interactions.....13
5.2. Effect of the defect dynamics.....15
5.3. Correlations 15

6. Summary and conclusions **18**
Acknowledgments **19**

References **19**

1. Introduction

The transportation is a universal phenomenon which occurs in a wide range of physical as well as biological processes, and it is currently a subject of intensive investigations [1]. Instances of such processes are traffic flow, pedestrian motion, cellular transport, protein synthesis and many more [1–5]. These processes show non-zero particle currents, which categorizes them as non-equilibrium. In the cellular world, biological molecular motors or motor proteins are known to play a special role in supporting the major functions such as cell motility, cell locomotion, cell division, and cargo transport along the filaments, etc [6–9]. In the intracellular transport, the motion of molecular motors carrying cargo is supported by the transformation of chemical energy derived from ATP hydrolysis into mechanical energy [2].

Recent *in vitro* experiments indicated that biological molecular motors that move along protein filaments interact with each other [10, 11]. Due to these short-range interactions, clusters of motor proteins can be formed, and this might influence their collective dynamics. In addition, while diffusing on cytoskeleton linear tracks biological motors might encounter other protein molecules bound to protein filaments that might interfere with their motion [12, 13]. These protein molecules can be viewed as

J. Stat. Mech. (2020) 043206

defects, and their effect on the multi-particle transport of molecular motors have been studied in recent years [14, 15]. One of the most important features of these defects is their dynamic nature, i.e. that they can stochastically bind and unbind from the linear tracks, and this should affect the movement of active motors [14]. There are several *in vivo* [16–18] and *in vitro* [19–22] experiments that observed the traffic jams in the transport of molecular motors due to the presence of microtubule-associated proteins (MAPs). An overview of different types of defects and their effects on molecular motor movement is represented in tabular form in [14]. In addition, the cytoskeleton motor proteins that move along cytoskeleton protein filaments can be divided into two groups depending on their processivity [2]. Processive motors, like conventional kinesins and myosins-V, can make hundreds of steps before dissociating from the filament tracks, while non-processive motors, like NCD kinesins and myosins-II, can make only few steps before dissociating back into the solution. In this case, the non-processive motors might be viewed as defects for the transport of processive molecular motors.

To explain multi-particle transport phenomena in natural systems, one frequently uses a class of non-equilibrium models known as totally asymmetric simple exclusion processes (TASEP) [1]. It was originally proposed as a model to describe the kinetics of biopolymerization [23]. Later, it was generalized to describe the biological transport processes, in particular the motion of molecular motors [1]. The simplest version of TASEP considers the active species as point particles that hop unidirectionally and stochastically in one preferred direction on a homogeneous one-dimensional (1D) lattice. In contrast to periodic boundary conditions, when the two ends of lattice are connected to a reservoir of infinite particles (open boundary conditions (OBC)), which seems to be a more realistic description of real dynamic processes, the model reveals interesting phenomena such as phase separations, phase segregation and boundary induced phase transitions [1, 24–28].

TASEP can be solved exactly only for homogeneous systems without interactions [24, 25, 27]. More complex multi-particle non-equilibrium processes are frequently analysed using simple mean-field approaches that neglect correlations in such systems [1, 29]. But adding the inter-molecular interactions introduces significant correlations, and this leads to the failure of the simple mean-field methods. To resolve this issue, a cluster mean-field (CMF) approach that accounts for some correlations has been introduced [30] and successfully utilized for analysing various molecular motors systems [31, 32]. Furthermore, several generalizations of TASEP have been employed for uncovering collective dynamics of biological molecular motors in more realistic circumstances. Examples include the investigation on the role of local inhomogeneity [29], the effect of dynamic blockages where the particles are completely blocked from the forward motion if the defect is sitting at the specific site [33], the role of association/dissociation kinetics of defect particles with diffusive and non-diffusive characteristics [34], and the reversible transformation to a local disordered state that can hinder the movement of particles [35].

Inspired by the realistic features of the transport of biological molecular motors along linear filaments, in this paper we aim to analyse the effect of stochastic binding and unbinding events of the defect particle on dynamics of interacting molecular motors. More specifically, we are stimulated by observations that the dynamics of processive cytoskeleton motor proteins can be affected by the presence of other

J. Stat. Mech. (2020) 043206

non-processive proteins. Our goal is to investigate the coupling between the association/dissociation dynamics of the defect and the inter-molecular interactions. Since the defect introduces the inhomogeneity in the system, simple mean-field approaches cannot be utilized here. We generalize a CMF approach that allows us to comprehensively describe the stationary properties of the system. It is found that there are only three or less possible stationary phases in the system, and one one of them is strongly affected by the defect dynamics. Our theoretical calculations are supported by extensive Monte Carlo computer simulations.

2. Definition of the model

The main goal of the proposed model is to investigate a TASEP model for interacting particles with the addition of binding/unbinding kinetics of the defect particle at the specific location. We consider a 1D lattice with N sites, as shown in figure 1, where the moving particles obey hard core exclusion principle. The particle are allowed to enter the system from the left and the particle leaves the lattice from the last site: see figure 1. All particles are identical and move along the lattice in one preferred direction (to the right).

It is also assumed that there is another type of particle, called a defect, that is allowed to bind to a special site k far away from the boundaries. To simplify the analysis, we neglect the interactions between the defect particle and the molecular motors because these species are different. But the potential interactions between these two different types of particles can be considered by extending the proposed theoretical method. For our analysis, we set the special site to be $k = N/2$, and the defect binds to the lattice with a rate $k_{\rm on}$ if it is free from the defect and it unbinds with a rate $k_{\rm off}$—see figure 1(C). Although the transition rates of the defect at $i = k$ are not altered by the presence of particles, the presence of the defect modifies the hopping rates of the particles from the site $(k-1)$ to the site k. The particle jumps with a reduced rate $p_d \leqslant 1$ from $(k-1)$th site to kth site if the defect is present, and otherwise the hopping rate is 1. For the case $p_d = 0$ the effect of the defect is the strongest, while for $p_d = 1$ the particles do not feel the presence of the defect at all. If the particle and the defect both are present at the site k, the hopping rate of the particle to $(k+1)$th site remains 1. Since the particles and the defect are two different species, we denote τ_i and σ_k as their respective occupation numbers. These occupation numbers τ_i and σ_k takes two values 1 or 0, which represents the presence or absence of a particle at site i and defect at the site k, respectively. It should be noted that the parameter p_d reflects the real structures of the cytoskeleton protein filaments that differ from the simplified 1D picture presented above [2, 6]. For example, microtubules can be viewed as several parallel protofilaments assembled together in a cylindrical fashion. Then the defect protein can be found at one of the protofilaments, while the molecular motor can be found on the neighboring protofilament. In this case, the molecular motor can move forward but it should also feel the presence of the defect particle in passing near it.

It has been experimentally observed that the molecular motors interact with each other, and these interactions are short-ranged, effectively creating inter-molecular

J. Stat. Mech. (2020) 043206

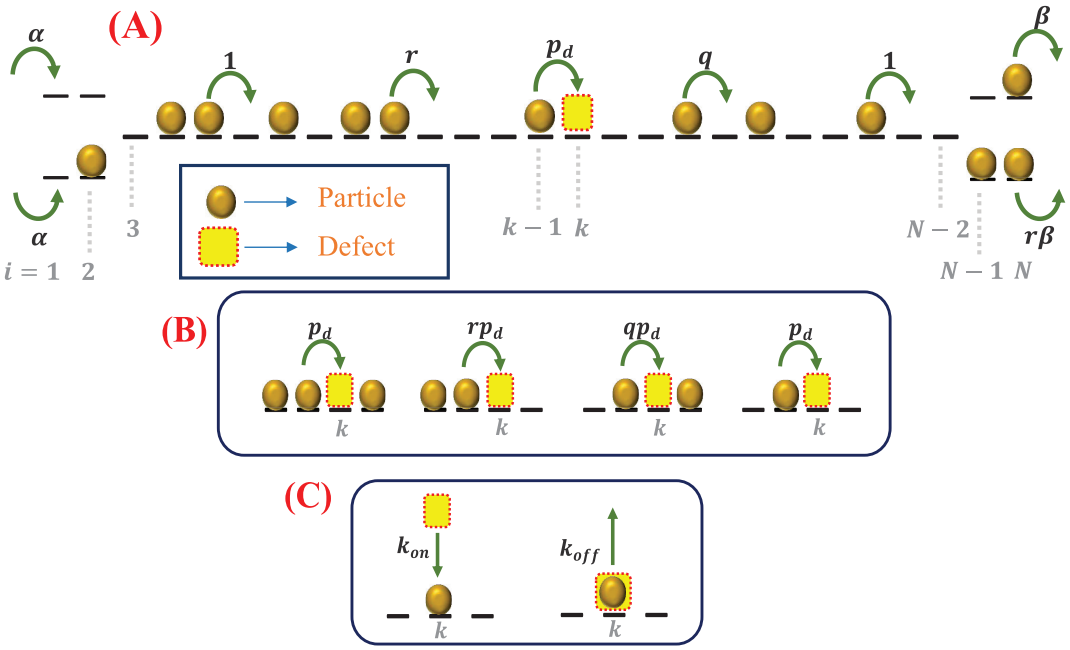

Figure 1. (A) A schematic view of the TASEP model for interacting particles with a dynamic defect. Circle are particles moving from the left to right. Square describes the defect siting at the site k. (B) The transition rates of the particle when it moves from the site $i = (k-1)$ to the site $i = k$ with a rate $p_d < 1$ because the defect is at the site k. (C) The binding and unbinding rates for the defect at the site k, which is independent of the particle occupation of this site.

bonds between particles [10, 11]. The formation and breaking of these bonds can be described using transition rates q and r, respectively, that depend on the energy E (in $k_{\mathrm{B}}T$ units) of inter-molecular interactions. Here, the positive ($E > 0$) energy represents attractive and the negative ($E < 0$) energy depicts repulsive interactions between the motors. One could introduce a thermodynamically consistent description of the transitions rates q and r [32, 36–38]. Then these rates can be written as

$$q = \exp[\theta E], \quad r = \exp[(\theta - 1)E] \tag{1}$$

where θ is a splitting factor that lies within the range $[0, 1]$ and it specifies how the interaction energy affects separately the formation and breaking the bonds. From this point of view, the formation and breaking of the bond is considered as a reversible chemical reaction with chemical equilibrium constant given by $K = q/r$ [8]. Since the interactions are short-ranged, if the hopping of particle leads to the bond formation (breaking) with the neighboring particle, the corresponding transition rate is q (r). Whereas, if bond formation and breaking occurs simultaneously the hopping rate is 1, as illustrated in figure 1(A).

In the presence of the defect at the site k, the transition rate for the particle from the site $k-1$ to the site k is modified due to inter-molecular interactions as shown in figure 1(B). If the site $k-2$ is occupied (empty) and the site $k+1$ is empty (occupied) the particle hops with the rate rp_d (qp_d). Whereas, if both the neighboring sites are occupied or empty simultaneously, the particle hops with the rate p_d: see figure 1(B). Interactions also change the entry and the exit rates of the particles. The particle

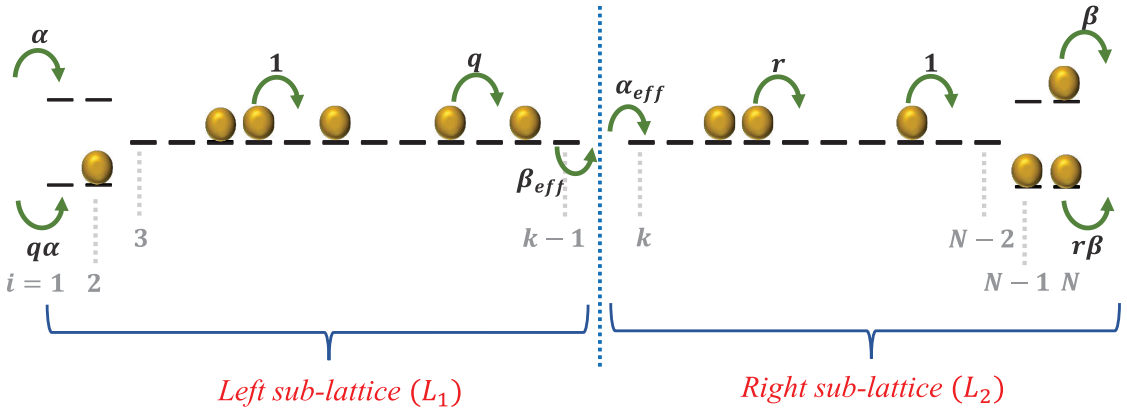

Figure 2. The division of the original inhomogeneous system into two coupled homogeneous segments: the left sub-lattice L_1 ($i = 1$ to $(k-1)$) and the right sub-lattice L_2 ($i = k$ to N). The effective exit rate from L_1 is β_{eff} and the effective entry rate into L_2 is α_{eff}.

attempts to enter the lattice with a rate $q\alpha$ if the second site ($i = 2$) is occupied as it leads to the formation of the inter-molecular bond. The entrance rate is α if the second site is empty. If the site previous to last site ($i = N-1$) is occupied, the particle leaves the lattice by breaking the bond with a rate $r\beta$, otherwise the exit rate is β.

To analyse better our inhomogeneous system, we divide the lattice in two homogeneous sub-lattices L_1 and L_2 as shown in figure 2. The left sub-lattice L_1 describes the lattice segment from the site $i = 1$ to the site $i = k-1$, and the right sub-lattice describes the lattice segment from the site $i = k$ to the site $i = N$. The homogeneous TASEP for interacting particles has been already extensively studied: see [32, 36–38]. In our theoretical framework, one needs to introduce the effective exit rate of the particles from L_1 as β_{eff} and the effective entry rate of the particle to L_2 as α_{eff}. These quantities are unknown and need to be evaluated. The two sub-lattices are coupled in the steady-state regime because the same particle currents must pass each sub-lattice. This allows us to calculate α_{eff} and β_{eff}, providing a convenient way of explicitly investigating the dynamical properties of the TASEP model with interacting particles and with the dynamic defect.

3. Mathematical description of the model

Dynamic properties of homogeneous TASEP for the particles with only hard-core exclusions has been well studied using exact and simple mean-field approaches [24, 25, 27]. It was found that there exist three distinct stationary phases: low-density (LD), high density (HD) and maximal current (MC). Adding short-range interactions to particles make the corresponding TASEP models too complex to be solved exactly, and it was also argued that simple mean-field approaches fail for these systems. However, the CMF methods that take into account some correlations are able to correctly describe the complex dynamics in the TASEP model for interacting molecules [32, 36–38]. Theoretical calculations show that the original LD, HD and MC stationary phases

J. Stat. Mech. (2020) 043206

remain intact, and only the boundaries between phases change with varying the interaction energy E. It seems reasonable to apply the CMF method for our system too. Let us first review the main results from the CMF theoretical approach.

3.1. Two-site CMF approximation for TASEP with interacting particles

The main assumption of the two-site CMF approximation is that the probability of the cluster of n sites $P(\tau_i, \tau_{i+1}, \ldots, \tau_n)$ is proportional to the product of probabilities of two-site clusters,

$$P(\tau_i, \tau_{i+1}, \ldots, \tau_n) \propto P(\tau_i, \tau_{i+1})P(\tau_{i+1}, \tau_{i+2}) \ldots P(\tau_{n-1}, \tau_n), \tag{2}$$

which undergoes normalization and eventually yields,

$$P(\tau_i, \tau_{i+1}, \ldots, \tau_n) = \frac{P(\tau_i, \tau_{i+1})P(\tau_{i+1}, \tau_{i+2}) \ldots P(\tau_{n-1}, \tau_n)}{P(\tau_{i+1})P(\tau_{i+2}) \ldots P(\tau_{n-1})}. \tag{3}$$

The probabilities for four possible states of any two-site cluster are the following: $P(1,1)$ when both sites are occupied by the particles; $P(1,0)$, $P(0,1)$ when only one site is occupied; and $P(0,0)$ when both sites are empty. For simplicity we denote $x \equiv P(1,1)$, $z \equiv P(0,0)$ and due to particle-hole symmetry $y \equiv P(1,0) = P(0,1)$. Now, we can calculate the bulk particle current in the system,

$$\begin{aligned} J_{\text{bulk}} = \langle (1-\tau_{i-1})\tau_i(1-\tau_{i+1})(1-\tau_{i+2})\rangle + q\langle (1-\tau_{i-1})\tau_i(1-\tau_{i+1})\tau_{i+2}\rangle \\ + r\langle \tau_{i-1}\tau_i(1-\tau_{i+1})(1-\tau_{i+2})\rangle + \langle \tau_{i-1}\tau_i(1-\tau_{i+1})(\tau_{i+2})\rangle. \end{aligned} \tag{4}$$

The currents at the entry and at the exit site are written as

$$J_{\text{entr}} = \alpha\left[\langle (1-\tau_1)(1-\tau_2)\rangle + q\langle (1-\tau_1)\tau_2\rangle\right], \tag{5}$$

$$J_{\text{exit}} = \beta\left[\langle (1-\tau_{N-1})\tau_N\rangle + r\langle \tau_{N-1}\tau_N\rangle\right]. \tag{6}$$

The average particle density at the site i is denoted as $\langle \tau_i \rangle \equiv \rho_i$, and since the density is uniform for the homogeneous lattice the subscript i can be dropped. Furthermore, employing the two-site CMF in the thermodynamic limit $N \to \infty$, equations (4)–(6) reduce to [32],

$$J_{\text{bulk}} = \frac{y^2 z + q y^3 + r x y z + x y^2}{\rho(1-\rho)}, \tag{7}$$

$$J_{\text{entr}} = \alpha(z + qy), \tag{8}$$

$$J_{\text{exit}} = \beta(y + rx). \tag{9}$$

To compute the current in the system, we need to calculate x, y and z which can be evaluated by using the Kolmogorov conditions;

$$x + y = \rho, \tag{10}$$

$$y + z = 1 - \rho. \tag{11}$$

We can also use the master equation for the density of the half-filled clusters, $y \equiv P(1,0)$, leading to [32, 38]

$$y = \sqrt{\frac{rxz}{q}}. \tag{12}$$

Solving equations (10)–(12) gives the explicit expressions for the three probabilities of different clusters in terms of the particle density and interactions:

$$x = \begin{cases} \frac{1}{2}\left(2\rho + \frac{r-\sqrt{r(r+4(q-r)\rho(1-\rho))}}{q-r}\right), & q, r \neq 1 \\ \rho^2, & q = r = 1. \end{cases} \tag{13}$$

$$y = \begin{cases} \frac{-r+\sqrt{r(r+4(q-r)\rho(1-\rho))}}{2(q-r)}, & q, r \neq 1 \\ \rho(1-\rho), & q = r = 1. \end{cases} \tag{14}$$

$$z = \begin{cases} \frac{1}{2}\left(2(1-\rho) + \frac{r-\sqrt{r(r+4(q-r)\rho(1-\rho))}}{q-r}\right), & q, r \neq 1 \\ (1-\rho)^2, & q = r = 1. \end{cases} \tag{15}$$

Substituting these expressions into equations (7)–(9), we can evaluate the bulk densities in the LD and the HD phases using the current continuity condition $J_{\text{entr}} = J_{\text{bulk}}$ and $J_{\text{exit}} = J_{\text{bulk}}$ respectively [32, 36–38]. The bulk density in the MC phase is equal 0.5, which is obtained from the condition $\frac{\partial J}{\partial \rho} = 0$. Moreover, the regions in which the different phases exist have been calculated [32]. The LD and HD phase exist for parameters that satisfies $\alpha < \frac{\beta}{\sqrt{q/r}}$, $\alpha < \alpha_c$ and $\alpha > \frac{\beta}{\sqrt{q/r}}$, $\beta < \beta_c$, respectively. The parameters α_c and β_c can be found using the relation $J_{\text{LD}} = J_{\text{MC}}$ and $J_{\text{HD}} = J_{\text{MC}}$. Finally, the MC phase is found for $\alpha > \alpha_c$, $\beta > \beta_c$.

3.2. Defect dynamics

Now let us consider the dynamics of the defect at the site k. The temporal evolution of the defect density at the site k can be presented as

$$\frac{\mathrm{d}\langle\sigma_k\rangle}{\mathrm{d}t} = k_{\text{on}}\langle(1-\sigma_k)\rangle - k_{\text{off}}\langle\sigma_k\rangle. \tag{16}$$

Writing $\langle\sigma_k\rangle \equiv \rho^*$ (the average occupation fraction of the defect), in steady state conditions equation (16) reduces to

$$\rho^* = \frac{k_{\text{on}}}{k_{\text{on}} + k_{\text{off}}}. \tag{17}$$

For the case when no defect can bind to the protein filament, we have $k_{\text{on}} = 0$ and it yields $\rho^* = 0$. It reduces the proposed model to the homogeneous interacting molecular motors model that have been investigated in detail before [32]. However, due to defect the dynamics in our system differs from the fully homogeneous case. The lattice can now be divided into two sub-lattices, the current from the site $(k-1)$ to the site k couples the sub-lattices L_1 and L_2, and it can be written as

J. Stat. Mech. (2020) 043206

$$J_{\text{coupling}} = \rho^* J^d + (1-\rho^*)\bar{J}^d. \tag{18}$$

Here, J^d and $\bar{J}^d$ defines the current in the presence and absence of defect at the site k, respectively. The parameters ρ^* and $(1-\rho^*)$ give the probability of the site k being occupied by the defect or to be empty, respectively. It can be shown that

$$\bar{J}^d = \Big(\langle(1-\tau_{k-2})\tau_{k-1}(1-\tau_k)(1-\tau_{k+1})\rangle + q\langle(1-\tau_{k-2})\tau_{k-1}(1-\tau_k)\tau_{k+1}\rangle + r\langle\tau_{k-2}\tau_{k-1}(1-\tau_k)(1-\tau_{k+1})\rangle + \langle\tau_{k-2}\tau_{k-1}(1-\tau_k)(\tau_{k+1})\rangle\Big). \tag{19}$$

To simplify calculations, we ignore all defect-particle and particle–particle interactions for the four consecutive sites $i = (k-2)$, $(k-1)$, k and $(k+1)$. Now, denoting $\langle\tau_{k-2}\rangle \equiv \rho_{b,1}$ and $\langle\tau_k\rangle \equiv \rho_{b,2}$, equation (19) reduces to

$$\bar{J}^d = \Big(\rho_{k-1}(1-\rho_k)\Big)\Big((1-\rho_{b,1})(1-\rho_{b,2}) + q(1-\rho_{b,1})\rho_{b,2} + r\rho_{b,1}(1-\rho_{b,2}) + \rho_{b,1}\rho_{b,2}\Big), \tag{20}$$

where $\rho_{b,1}$ and $\rho_{b,2}$ represents bulk density in the left and in the right sub-lattices L_1 and L_2, respectively. In the presence of the defect, the particle current is simply written as

$$J^d = p_d \bar{J}^d. \tag{21}$$

When the rate $p_d = 1$ equation (18) gives $J_{\text{coupling}} = J^d$, and the model is identical to the fully homogeneous case that was investigated in [31, 32]. Hence, it is interesting to investigate when $p_d \neq 1$ since this will exhibit the role of the defect at the site k. Under the mean-field approximation, the current at the exit site of the left sub-lattice L_1 and at the entrance site of the right sub-lattice L_2 are given by

$$J_{\text{exit},1} = \beta_{\text{eff}}\rho_{k-1}[1 + (r-1)\rho_{b,1}], \tag{22}$$

$$J_{\text{entr},2} = \alpha_{\text{eff}}(1-\rho_k)[1 + (q-1)\rho_{b,2}]. \tag{23}$$

The expression for β_{eff} can be computed by equating the current leaving the left sub-lattice L_1 to the coupling current $J_{\text{exit},1} = J_{\text{coupling}}$, producing

$$\beta_{\text{eff}} = (1 + (p_d - 1)\rho^*)\Big(\frac{\rho_{k-1}(1-\rho_k)}{\rho_{k-1}(1+(r-1)\rho_{b,1})}\Big)\Big((1-\rho_{b,1})(1-\rho_{b,2}) + q(1-\rho_{b,1})\rho_{b,2} + r\rho_{b,1}(1-\rho_{b,2}) + \rho_{b,1}\rho_{b,2}\Big). \tag{24}$$

Similarly, α_{eff} is evaluated by equating the entrance current into L_2 with the coupling current $J_{\text{entr},2} = J_{\text{coupling}}$,

$$\alpha_{\text{eff}} = (1 + (p_d - 1)\rho^*)\Big(\frac{\rho_{k-1}(1-\rho_k)}{(1-\rho_k)(1+(q-1)\rho_{b,2})}\Big)\Big((1-\rho_{b,1})(1-\rho_{b,2}) + q(1-\rho_{b,1})\rho_{b,2} + r\rho_{b,1}(1-\rho_{b,2}) + \rho_{b,1}\rho_{b,2}\Big). \tag{25}$$

The above expressions will be further utilized to compute the properties of the system such as phase diagrams, density profiles and correlations.

4. Stationary phase diagrams

Because each homogeneous TASEP can have one of three phases (LD, HD or MC), our inhomogeneous system consisting of two coupled homogeneous sub-lattices can have upto 9 possible stationary phases [32]. At the steady-state conditions, we have

$$J_{\text{bulk},1} = J_{\text{bulk},2}, \tag{26}$$

where $J_{\text{bulk},1}$ and $J_{\text{bulk},2}$ represent the bulk currents in L_1 and L_2, respectively, which can be explicitly obtained from equation (7) with the corresponding probabilities of the clusters x_j, y_j and z_j ($j = 1$ for L_1 and $j = 2$ for L_2).

The condition in equation (26) implies that

$$\rho_{b,1} = \rho_{b,2}, \tag{27}$$

$$\text{or} \qquad \rho_{b,1} + \rho_{b,2} = 1. \tag{28}$$

Then the possibility of having the MC phase in any of the sub-lattices and the LD or the HD phase in the other sub-lattice can be discarded because these phases support different particle currents. Hence, this leaves only 5 possible stationary phases, namely: LD/LD, HD/HD, MC/MC, HD/LD and LD/HD. In this notation, the first term corresponds to the state of the segment L_1, while the second term describes the segment L_2. Moreover, equation (27) states that in the case of LD/LD, HD/HD and MC/MC phases the density in both sub-lattices will be equal. Now, let us explore the conditions for existence of these possible phases.

4.1. HD/LD phase

This phase is determined by the occupation fractions of the exit site on left sub-lattice ($\rho_{k-1} = \rho_{b,1}$) and the entry site on the right sub-lattice ($\rho_k = \rho_{b,2}$). This phase exists if the entry and the exit rates satisfy the following conditions:

$$\alpha > \frac{\beta_{\text{eff}}}{\sqrt{q/r}}, \quad \beta_{\text{eff}} \leqslant \beta_c, \tag{29}$$

$$\alpha_{\text{eff}} < \frac{\beta}{\sqrt{q/r}}, \quad \alpha_{\text{eff}} \leqslant \alpha_c \tag{30}$$

where α_c and β_c are the coordinates of the triple point for the system. The current continuity condition at the entrance of the right sub-lattice helps us to calculate the bulk density $\rho_{b,2}$,

$$\alpha_{\text{eff}}(z_2 + qy_2) = \frac{y_2^2 z_2 + q y_2^3 + r x_2 y_2 z_2 + x_2 y_2^2}{\rho_{b,2}(1 - \rho_{b,2})} \tag{31}$$

where α_{eff} is unknown. The density $\rho_{b,1}$ is evaluated using equation (34). Utilizing above equations along with equations (24) and (25), the effective entrance and exit rates, α_{eff} and β_{eff} are explicitly found. It can be also shown that $\alpha_{\text{eff}} = \alpha_c$ and $\beta_{\text{eff}} = \beta_c$.

J. Stat. Mech. (2020) 043206

4.2. LD/LD phase

This phase is governed by the following condition,

$$\alpha < \frac{\beta_{\text{eff}}}{\sqrt{q/r}}, \quad \alpha \leqslant \alpha_c, \tag{32}$$

$$\alpha_{\text{eff}} < \frac{\beta}{\sqrt{q/r}}, \quad \alpha_{\text{eff}} \leqslant \alpha_c. \tag{33}$$

In this phase, the bulk density in L_1 ($\rho_{b,1}$) and L_2 ($\rho_{b,2}$) is determined by the entry site occupation of the left sub-lattice and the right sub-lattice, respectively. Utilizing the current continuity condition, $\rho_{b,1}$ is obtained by equating the current at the entrance of the left sub-lattice to that in the bulk of L_1 for known value of α, yielding

$$\alpha(z_1 + qy_1) = \frac{y_1^2 z_1 + q y_1^3 + r x_1 y_1 z_1 + x_1 y_1^2}{\rho_{b,1}(1 - \rho_{b,1})}, \tag{34}$$

where x_1, y_1 and z_1 are obtained from equations (13)–(15) for $\rho = \rho_{b,1}$. Furthermore, using the relation $J_{\text{exit},1} = J_{\text{bulk},1}$ the density at the exit site of L_1 is given by;

$$\rho_{k-1} = \frac{J_{\text{bulk},1}}{\beta_{\text{eff}}(1 + (r-1)\rho_{b,1})}. \tag{35}$$

Now, for the right sub-lattice, the density $\rho_{b,2}$ is given by

$$\alpha_{\text{eff}}(z_2 + qy_2) = \frac{y_2^2 z_2 + q y_2^3 + r x_2 y_2 z_2 + x_2 y_2^2}{\rho_{b,2}(1 - \rho_{b,2})} \tag{36}$$

where α_{eff} is still unknown. Hence, we need to compute α_{eff} and β_{eff} by solving the system of non-linear equations (24), (25), (35) and (36) for known values of E, k_{on}, k_{off} and p_d. We can also show that the bulk densities in both lattices satisfy equation (27). The obtained values of α_{eff} and β_{eff} are used then to determine the boundaries of this phase from the conditions presented in equations (32) and (33).

4.3. HD/HD phase

The conditions for the existence of this phase are

$$\alpha > \frac{\beta_{\text{eff}}}{\sqrt{q/r}}, \quad \beta_{\text{eff}} \leqslant \beta_c, \tag{37}$$

$$\alpha_{\text{eff}} > \frac{\beta}{\sqrt{q/r}}, \quad \beta \leqslant \beta_c. \tag{38}$$

In this phase, the dynamics in the two sub-lattices L_1 and L_2 is governed by the exit sites on the respective lattices. Starting with the known value of β, and using

$$\beta(y_2 + rx_2) = \frac{y_2^2 z_2 + q y_2^3 + r x_2 y_2 z_2 + x_2 y_2^2}{\rho_{b,2}(1 - \rho_{b,2})} \tag{39}$$

J. Stat. Mech. (2020) 043206

we calculate $\rho_{b,2}$. Employing $J_{\text{entr},2} = J_{\text{bulk},2}$, the density at the entry site of L_2 is given by

$$\rho_k = \frac{J_{\text{bulk},2}}{\alpha_{\text{eff}}(1 + (q-1)\rho_{b,2})}, \tag{40}$$

where α_{eff} is unknown. The bulk density in the left sub-lattice L_1, is obtained from

$$\beta_{\text{eff}}(y_1 + rx_1) = \frac{y_1^2 z_1 + q y_1^3 + r x_1 y_1 z_1 + x_1 y_1^2}{\rho_{b,1}(1-\rho_{b,1})}, \tag{41}$$

where β_{eff} is unknown. So, we have a coupled system of equations (24), (25), (40) and (41) that can be numerically solved to find the rates α_{eff} and β_{eff} for specific values of E, k_{on}, k_{off} and p_d. Correspondingly, the HD/HD phase can be obtained for the values α, β, α_{eff} and β_{eff} satisfying equations (37) and (38).

4.4. LD/HD phase

This phase exists when the following conditions are satisfied,

$$\alpha < \frac{\beta_{\text{eff}}}{\sqrt{q/r}}, \quad \alpha \leqslant \alpha_c, \tag{42}$$

$$\alpha_{\text{eff}} > \frac{\beta}{\sqrt{q/r}}, \quad \beta \leqslant \beta_c. \tag{43}$$

The bulk densities in the left and the right sub-lattices ($\rho_{b,1}$ and $\rho_{b,2}$) are calculated using equations (34) and (39), respectively, for known values of α and β. These parameters are further utilized in equations (24), (25), (35) and (40) to compute the effective rates α_{eff} and β_{eff}. Our specific calculations found that there are no parameters (α, β, α_{eff} and β_{eff}) that could satisfy equations (42) and (43). Hence, the conditions for the existence of LD/HD phase are violated, and this phase cannot be realized at all.

4.5. MC/MC phase

In this phase, the bulk densities in each sub-lattice must be equal to 0.5, independently of the values of α, β and the effective entry and exit rates. The conditions the existence of this phase are given by

$$\alpha \geqslant \alpha_c, \quad \beta_{\text{eff}} \geqslant \beta_c, \tag{44}$$

$$\alpha_{\text{eff}} \geqslant \alpha_c, \quad \beta \geqslant \beta_c. \tag{45}$$

We found that here also does not exist any set of parameters that could satisfy all the above conditions simultaneously. This phase can exist only when there is no inhomogeneity in the system, i.e. for $\rho^* = 0$. Thus, for general situations with the defect this phase also cannot be found at stationary conditions.

Explicitly checking the conditions for existence of all possible phases, we found that the system can support only 3 stationary phases: LD/LD, HD/LD and HD/HD.

J. Stat. Mech. (2020) 043206

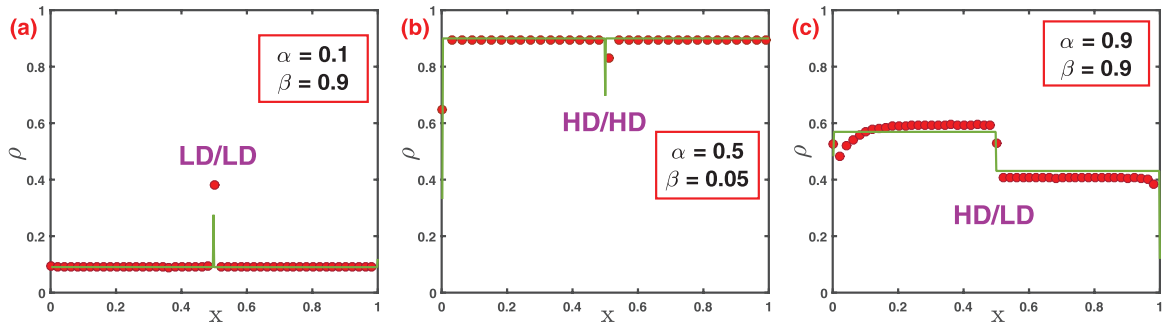

Figure 3. Density profiles for three different stationary phases. In all cases we utilized: $p_d = 0.1$, $E = -1.6\ k_BT$ and $\theta = 0.5$. (a) LD/LD phase with $k_{on} = 0.9$ and $k_{off} = 0.3$; (b) HD/HD phase with $k_{on} = 0.9$ and $k_{off} = 0.3$; (c) HD/LD phase with $k_{on} = 0.2$ and $k_{off} = 0.6$. Solid green lines correspond to numerically exact two-site CMF calculations and red symbols represent the Monte Carlo simulations.

5. Results and discussions

The dynamics in the system is governed by four main parameters: interaction energy E, the defect association rate k_{on}, the defect dissociation rate k_{off} and the defect-particle interaction parameter p_d that specifies how the transition rates of the particle change if the defect is present at the special site k. Now let us investigate in detail the role of each of these parameters.

To test the validity of our theoretical method, the approximated results obtained in the previous section are probed with extensive Monte Carlo simulations. For simulations, the random sequential update rules are followed with lattice length $N = 1000$ and the simulation is allowed to run for 2×10^9 time steps to attain a steady-state. The dynamics of defect is considered to be at $k = N/2$. While simulating, if the site k is found to be occupied with both the defect and the particle, we preferred the detachment of the defect rather than the jump of particle. To ensure the occurrence of steady state, first 5% of the total number of time steps are ignored.

Figure 3 shows the comparison of our theoretical calculations for density profiles with the results of computer simulations. One can see that that our method describes reasonably well all different stationary phases. This suggests that we can now specifically study the role of various factors in the dynamics of interacting particles in the presence of the dynamic defect.

5.1. Effect of interactions

Interaction energy E is the measure of the tendency to form inter-molecular bonds. For $E < 0$, the particles repel each other and they do not like to form the bond. But for $E > 0$, the particle clusters are easily formed. We calculated stationary phases for different interactions energies, and results are presented in figures 4 and 5. One can see that 3 stationary phases exist for weak repulsions ($E = -1.6\ k_BT$, figure 4(a)), and increasing the repulsion have a strong effect on the stationary dynamics. Below the critical value $E_c \simeq -2.6\ k_BT$, the HD/LD phase completely disappears (figure 4(b)). At the same time, the LD/LD phase significantly increases, while the HD/HD is getting

J. Stat. Mech. (2020) 043206

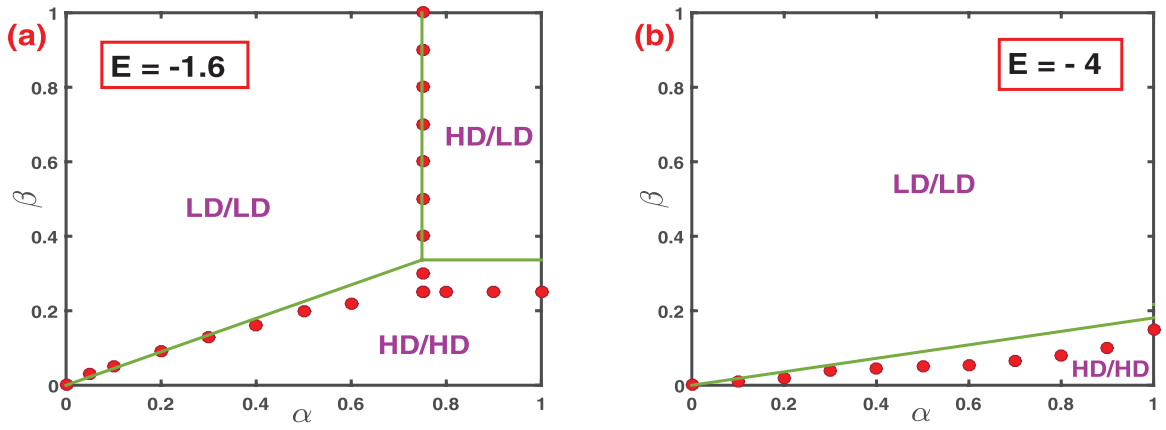

Figure 4. Stationary phase diagrams for $k_{\rm on} = 0.2$, $k_{\rm off} = 0.6$, $p_d = 0.1$, $\theta = 0.5$ and the interaction energy (a) $E = -1.6\ k_{\rm B}T$ and (b) $E = -4\ k_{\rm B}T$. Red symbols represent simulated results and solid green lines are the results from numerically exact calculations using two-site CMF.

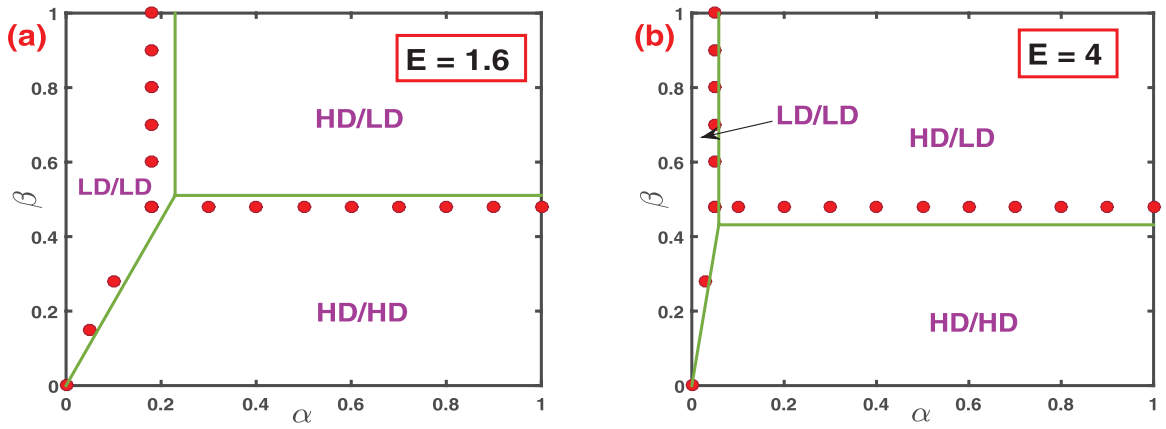

Figure 5. Stationary phase diagrams for $k_{\rm on} = 0.2$, $k_{\rm off} = 0.6$, $p_d = 0.1$, $\theta = 0.5$ and the interaction energy (a) $E = 1.6\ k_{\rm B}T$ and (b) $E = 4\ k_{\rm B}T$. Red symbols represent simulated results and solid green lines are the results from numerically exact calculations using two-site CMF.

smaller. These observations can be easily explained. Increasing repulsions stimulate particles to stay far way from each other, which can only be satisfied in LD phases. The stationary phases for attractive interactions show a slightly different picture. We again have 3 phases for weak attractions (figure 5(a)), while for strong attractions the LD/LD phase diminish and the HD/LD and HD/HD phases expand. These observations are expected since for attractive interactions particles tend to be closer with each other, which can be satisfied in high-density phases. We can clearly notice that these findings agree with the current views on mechanisms of interacting particles [31, 32]. One can also see from figures 4 and 5 that Monte Carlo computer simulations generally agree with our theoretical calculations for stationary phases.

J. Stat. Mech. (2020) 043206

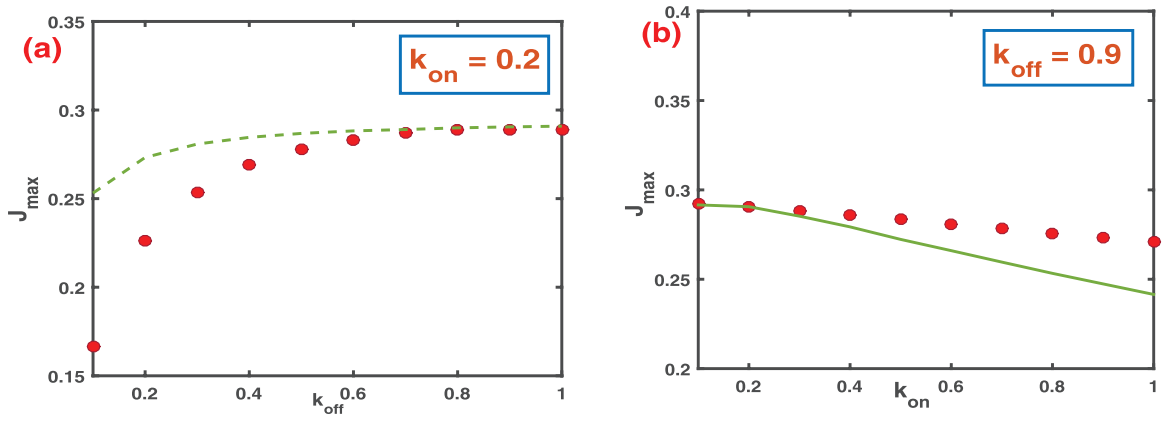

Figure 6. The dependence of the particle current $J_{\max}$ on the association/dissociation rates of the defect for $E = -1.6\ k_{\rm B}T$, $\theta = 0.5$ and $p_d = 0.1$; (a) fixed $k_{\rm on} = 0.2$ and $0 \leqslant k_{\rm off} \leqslant 1$; (a) fixed $k_{\rm off} = 0.9$ and $0 \leqslant k_{\rm on} \leqslant 1$. Green lines represent numerical results whereas symbols correspond to Monte Carlo computer simulations.

5.2. Effect of the defect dynamics

The defect is crucial for understanding the dynamics of particles in the system. When the defect is siting at the site k, the transition rates of the particles are locally affected. But the dynamics is normal and homogeneous when the the defect is not present at the special site. Our theoretical approach allows us to quantify the effect of the defect dynamics.

Figure 6 shows the dependence of the stationary currents on association and dissociation rates of the defect for weak repulsion ($E = -1.6\ k_{\rm B}T$) and for strong defect-particle interactions ($p_d = 0.1$). One can see that increasing the time when the defect is at the site k, which happens for smaller $k_{\rm off}$ and larger $k_{\rm on}$, decreases the particle current, as expected. The particles have difficulties to pass through the site k. Our theoretical method correctly predicts this effect, but it underestimates the effect of the dissociation rate and slightly overestimates the effect of association rate. This is clearly a consequence of neglecting the correlations near the special site k.

Varying the defect binding and unbinding rates has a limited effect on the phase diagrams of interacting particles, as illustrated in figure 7. Three stationary phase are always observed and only the boundaries between some phases are modified. Increasing the dissociation rate $k_{\rm off}$ or decreasing $k_{\rm on}$ generally expands the phase space occupied by the LD/LD phase, while the space for the HD/LD phase shrinks: see figure 7. Similar effects are observed for changing the defect-particle interactions, which can be done by varying the parameter p_d, as presented in figure 8.

5.3. Correlations

One of the most important features of the transport of interacting particles is the presence of correlations in the system. The CMF method can successfully describe the TASEP with interacting particles because it takes into account some of these correlations. We can quantify the effect of correlations by considering a function,

$$C_i = \langle \tau_i \tau_{i+1} \rangle - \langle \tau_i \rangle \langle \tau_{i+1} \rangle, \tag{46}$$

J. Stat. Mech. (2020) 043206

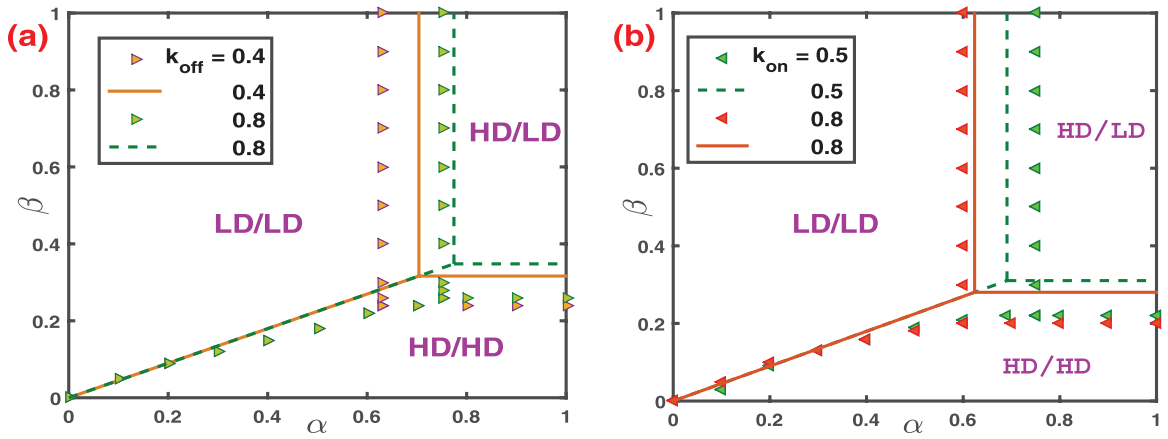

Figure 7. Stationary phase diagrams for $E = -1.6\ k_BT$, $\theta = 0.5$ and $p_d = 0.1$; (a) fixed $k_{on} = 0.2$ and $k_{off} = 0.4, 0.8$; (a) fixed $k_{off} = 0.9$ and $k_{on} = 0.5, 0.8$. Colored symbols represent the simulated results and the corresponding colored lines are numerically exact results using two-site CMF.

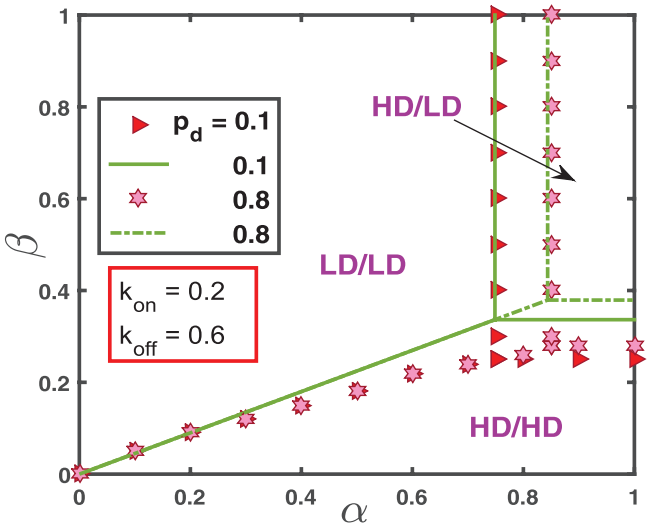

Figure 8. Stationary phase diagram for $k_{on} = 0.2$, $k_{off} = 0.6$, $E = -1.6\ k_BT$, $\theta = 0.5$ with varying the parameter p_d ($p_d = 0.1$ and $p_d = 0.8$ are considered). Red symbols correspond to simulated results and solid green lines are the results from numerically exact calculations using two-cluster CMF.

which can be explicitly evaluated in our theoretical approach. This allows us to understand where the presented theoretical method works better and why.

Figure 9 presents the particle density profiles and correlation profiles for the LD/LD and the HD/HD phases. In both cases, the correlations are relatively weak, and our theory can describe the dynamics perfectly well. There are only some deviations near the special site k, but they are quite local. Thus, the defect dynamics essentially does not affect the system in both these phases. This observation can be easily explained. In the LD/LD phase the rate-limiting step that determines the overall dynamics is the entrance into the system, while in the HD/HD phase the rate limiting step is the exit. Then the defect dynamics cannot influence the system beyond the small region near the special site.

J. Stat. Mech. (2020) 043206

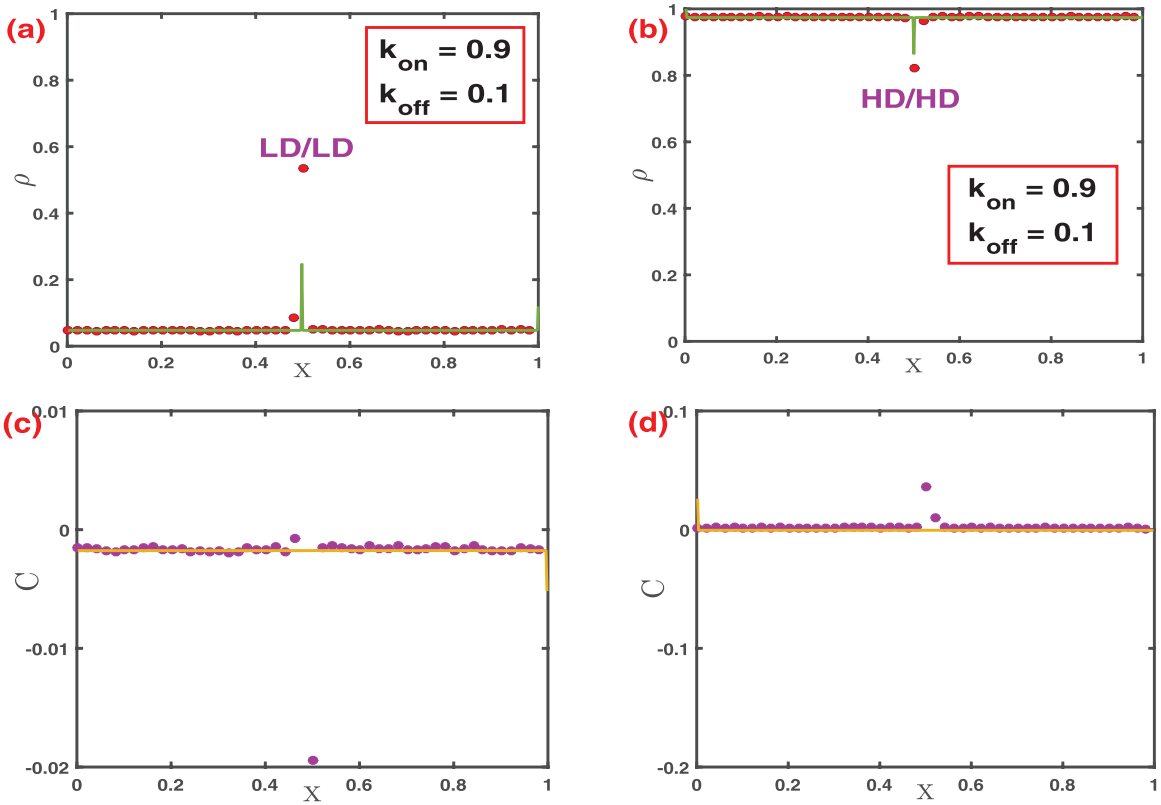

Figure 9. Correlations and particle densities for $k_{\rm on} = 0.9$, $k_{\rm off} = 0.1$, $p_d = 0.1$ and $\theta = 0.5$. (a) LD/LD phase density profile with $E = -1.6\ k_{\rm B}T$, $\alpha = 0.05$, and $\beta = 0.9$; (b) HD/HD density profile with $E = 1.6\ k_{\rm B}T$ $\alpha = 0.5$, and $\beta = 0.05$; (c) LD/LD correlation profile with $E = -1.6\ k_{\rm B}T$, $\alpha = 0.05$, and $\beta = 0.9$; (d) HD/HD correlation profile with $E = 1.6\ k_{\rm B}T$ $\alpha = 0.5$, and $\beta = 0.05$. Symbols correspond to Monte Carlo simulations and solid lines are due to our theoretical calculations.

However, as illustrated in figure 10, the situation is drastically different in the HD/LD phase. Our theory can only semi-quantitatively describe the density profiles in this phase (figures 10(a)–(c)). The discrepancy between theoretical predictions computer simulations growths up for larger $k_{\rm on}$ and smaller $k_{\rm off}$, i.e. for longer periods of the defect sitting at the site k and affecting the particle dynamics. In this phase, the amplitude of correlations is generally larger than in the LD/LD and HD/HD phases (figures 10(d)–(f)).While the correlations are decreasing for more active defect dynamics, our predictions are mainly quantitative in this case. We believe that the main reason for this is the mean-field assumption on the coupling between the sub-lattices. These arguments suggest that the defect is significantly influencing the dynamics in the HD/LD phase because the exit form the left sub-lattice and the entrance to the right sub-lattice are now rate-limiting steps. But both of them are strongly affected by the presence of the defect. This explains the role of the defect dynamics in the TASEP model of interacting particles.

J. Stat. Mech. (2020) 043206

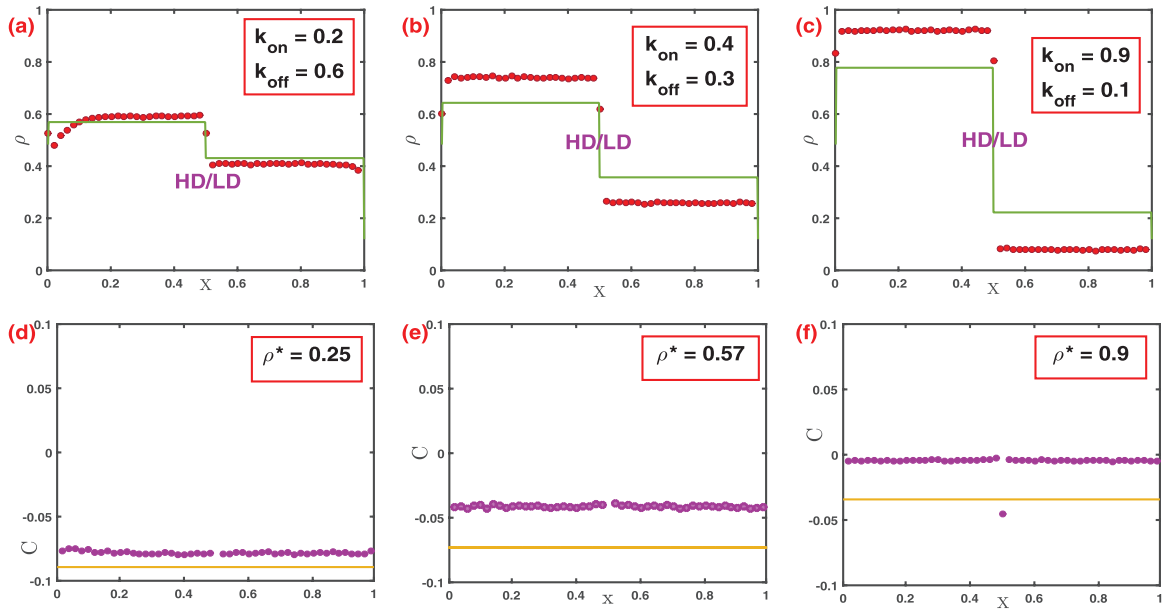

Figure 10. First row gives the density profiles for fixed parameters $\alpha = 0.9$, $\beta = 0.9$, $p_d = 0.1$, $E = -1.6\ k_BT$ and $\theta = 0.5$ with (a) $k_{on} = 0.2$ and $k_{off} = 0.6$; (b) $k_{on} = 0.4$ and $k_{off} = 0.3$; (c) $k_{on} = 0.9$ and $k_{off} = 0.1$. Green lines represent numerical results whereas red markers symbolize Monte Carlo simulations. Second row provides the correlation profiles for the same parameters in HD/LD phase where (d) is corresponding to (a) and (e) is corresponding to (b) and (f) is corresponding to (c). Yellow lines represent numerical results whereas pink symbols are Monte Carlo simulations.

6. Summary and conclusions

Stimulated by biological transport phenomena, a theoretical model is developed to analyse the dynamics of interacting molecular motors in the presence of dynamic defect that might slow down the particle flux. Our main finding is that the presence of the reversible dynamic defect does not change the number of possible stationary phases, although the nature of the dynamics is now different. It is determined by the sign and the strength of inter-molecular interactions, as well as the way the defect dynamics is coupled to the flux of translocating particles. In addition, the defect introduces correlations in the system that affect those stationary phases that are rate-limited by the process of passing the special site where the defect can be found.

More specifically, we generalized 1D totally asymmetric exclusion processes for interacting particles by including the effect of reversible defect. Since the model cannot be solved analytically and the simplest mean-field theoretical treatments cannot be used due to the neglect of correlations, we developed a CMF method to describe the dynamic processes in the system. The defect site introduces the inhomogeneity on the lattice, and we mapped our system into two coupled sub-lattices. This allows us to describe the dynamics of interacting particles at each homogeneous sub-lattice separately, and stationary conditions couple the currents between two parts of the system. Considering the dynamics at steady-state conditions, we determined that there are only three possible stationary phases found in the system. Two of them are governed by

J. Stat. Mech. (2020) 043206

the processes at the entrance or at the exit from the lattice, and for this reason they are not affected by the defect dynamics. However, the third one depends strongly on the details of binding and unbinding of the defect and also on how the presence of the defect modifies the flux of particles. Our theoretical predictions generally agree with results from Monte Carlo simulations, suggesting that our theoretical method correctly captures the physics of the process. We are also able to explain the deviations between theoretical calculations and computer simulations by connecting them to the neglect of correlations between two sub-lattices in the system.

The main goal of our theoretical analysis was to explain the dynamic features of the motor proteins, and the presented results were able to describe the effect of dynamic defects. However, our approach is rather oversimplified, and it neglects many features of the molecular motors cellular transport. For example, the motor proteins have extended sizes, there are many other molecules can be found on the protein filaments, and the cytoskeleton filaments frequently form networks. It will be important to take into account these more realistic features of the biological transport by employing more advanced theoretical methods.

Acknowledgments

ABK acknowledges the support from the Welch Foundation (Grant C-1559), from the NSF (Grant CHE-1664218) and from the Center for Theoretical Biological Physics sponsored by the NSF (Grant PHY-1427654).

References

[1] Chou T, Mallick K and Zia R 2011 *Rep. Prog. Phys.* **74** 116601
[2] Kolomeisky A B 2015 *Motor Proteins and Molecular Motors* (Boca Raton, FL: CRC Press)
[3] Foulaadvand M E and Maass P 2016 *Phys. Rev.* E **94** 012304
[4] Belitsky V, Krug J, Neves E J and Schütz G 2001 *J. Stat. Phys.* **103** 945–71
[5] Chowdhury D, Santen L and Schadschneider A 2000 *Phys. Rep.* **329** 199–329
[6] Howard J *et al* 2001 *Mechanics of Motor Proteins and the Cytoskeleton* (Sunderland, MA: Sinauer Associates)
[7] Bray D 2001 *Cell Movements: from Molecules to Motility* (New York: Garland)
[8] Kolomeisky A B and Fisher M E 2007 *Annu. Rev. Phys. Chem.* **58** 675–95
[9] Kolomeisky A B 2013 *J. Phys.: Condens. Matter* **25** 463101
[10] Chandel S, Chaudhuri A and Muhuri S 2015 *Europhys. Lett.* **110** 18002
[11] Roos W H, Campas O, Montel F, Woehlke G, Spatz J P, Bassereau P and Cappello G 2008 *Phys. Biol.* **5** 046004
[12] Dreblow K, Kalchishkova N and Böhm K J 2010 *Biochem. Biophys. Res. Commun.* **395** 490–5
[13] Seitz A, Kojima H, Oiwa K, Mandelkow E M, Song Y H and Mandelkow E 2002 *EMBO J.* **21** 4896–905
[14] Chai Y, Lipowsky R and Klumpp S 2009 *J. Stat. Phys.* **135** 241–60
[15] Grzeschik H, Harris R and Santen L 2010 *Phys. Rev.* E **81** 031929
[16] Bulinski J C, McGraw T E, Gruber D, Nguyen H L and Sheetz M P 1997 *J. Cell Sci.* **110** 3055–64
[17] Ebneth A, Godemann R, Stamer K, Illenberger S, Trinczek B, Mandelkow E M and Mandelkow E 1998 *J. Cell Biol.* **143** 777–94
[18] Sato-Harada R, Okabe S, Umeyama T, Kanai Y and Hirokawa N 1996 *Cell Struct. Funct.* **21** 283–95
[19] Hagiwara H, Yorifuji H, Sato-Yoshitake R and Hirokawa N 1994 *J. Biol. Chem.* **269** 3581–9
[20] Heins S, Song Y H, Wille H, Mandelkow E and Mandelkow E M 1991 *J. Cell Sci.* **1991** 121–4
[21] Lopez L A and Sheetz M P 1993 *Cell Motil. Cytoskeleton* **24** 1–16
[22] Paschal B M, Obar R A and Vallee R B 1989 *Nature* **342** 569
[23] MacDonald C T, Gibbs J H and Pipkin A C 1968 *Biopolymers* **6** 1–25

J. Stat. Mech. (2020) 043206

[24] Derrida B, Domany E and Mukamel D 1992 *J. Stat. Phys.* **69** 667–87
[25] Derrida B, Evans M R, Hakim V and Pasquier V 1993 *J. Phys. A: Math. Gen.* **26** 1493
[26] Krug J 1991 *Phys. Rev. Lett.* **67** 1882
[27] Schütz G and Domany E 1993 *J. Stat. Phys.* **72** 277–96
[28] Kolomeisky A B, Schütz G M, Kolomeisky E B and Straley J P 1998 *J. Phys. A: Math. Gen.* **31** 6911
[29] Kolomeisky A B 1998 *J. Phys. A: Math. Gen.* **31** 1153
[30] Schreckenberg M, Schadschneider A, Nagel K and Ito N 1995 *Phys. Rev.* E **51** 2939
[31] Teimouri H, Kolomeisky A B and Mehrabiani K 2015 *J. Phys. A: Math. Theor.* **48** 065001
[32] Celis-Garza D, Teimouri H and Kolomeisky A B 2015 *J. Stat. Mech.* P04013
[33] Sahoo M and Klumpp S 2016 *J. Phys. A: Math. Theor.* **49** 315001
[34] Sahoo M, Dong J and Klumpp S 2014 *J. Phys. A: Math. Theor.* **48** 015007
[35] Waclaw B, Cholewa-Waclaw J and Greulich P 2019 *J. Phys. A: Math. Theor.* **52** 065002
[36] Gomes L V and Kolomeisky A B 2017 *J. Phys. A: Math. Theor.* **51** 015601
[37] Midha T, Kolomeisky A B and Gupta A K 2018 *J. Stat. Mech.* 043205
[38] Midha T, Gomes L V, Kolomeisky A B and Gupta A K 2018 *J. Stat. Mech.* 053209

J. Stat. Mech. (2020) 043206